Brownian Motion and Thermophoresis Effects on Casson Nanofluid Over a Chemically Reacting Stretching Sheet with Inclined Magnetic Field

D. Gopal
Osmania University

N. Kishan
Osmania University

Gopal and Kishan: Brownian Motion and Thermophoresis Effects
Available at
http://pvamu.edu/aam
Appl. Appl. Math.
ISSN: 1932-9466

Applications and Applied Mathematics:
An International Journal
(AAM)

Brownian Motion and Thermophoresis Effects
on Casson Nanofluid Over a Chemically Reacting Stretching Sheet
with Inclined Magnetic Field

[1]**D. Gopal and** [2]**N. Kishan**

Department of Mathematics
Osmania University
Hyderabad, India 500007
[1]degavath.gopal@gmail.com, [2]kishan.naikoti@gmail.com

Abstract

The contemporary study explores the impact of thermophoresis and Brownian motion on two-dimensional magnetohydrodynamic boundary layer flow of Casson nanofluid over a chemically reacting stretching sheet. To control the heat and mass transport phenomena we also included the thermophoresis diffusion coefficient, Brownian motion parameter, and thermal radiation. The regular physical governing systems of partial differential equations are transmogrifying into ordinary differential equations. The transmogrifying governing equations are checked numerically by using Runge-Kutta-Fehlberg method. The numerical solutions for heterogeneous governing parameters such as Schmidt number, Joule heating parameter, and permeability parameter, chemical reaction parameters on velocity, temperature, and concentration profiles were presented. Numerical and Graphical results have described the parameters of concentration entering into the modeled problems. The analyzed numerical values of skin friction coefficient, Nusselt and Sherwood numbers also determined and chat about in the formal property of several assorted parameters.

Keywords: Brownian moment; thermophoresis; Casson fluid; chemical reaction; MHD; Joule heating; permeability parameter

MSC 2010 No.: 76A05, 58D30

1. Introduction

Analysis of non-Newtonian fluids is quite popular amongst the recent researchers. This is due to their occurrence in the industrial applications. There are several industrial and natural utilization

Applications and Applied Mathematics: An International Journal (AAM), Vol. 14 [2019], Iss. 4, Art. 9

AAM: Intern. J., Special Issue No. 4 (March 2019) 107

of such fluids, for volcanic lava, instance, molten polymers, paints, oils, drilling mud, polycrystal melts, fluid suspensions, cosmetic and food products and many others. The flow dynamics of non-Newtonian fluids can be described by nonlinear relationship between the shear stress and shear rate (Wang et al. (2011), Hayat al. (2017), Hsiao et al. (2017), Hayat et al. (2017), Khan et al. (2017), Hsiao et al. (2017) and Khan et al. (2017)). Further, these fluids have shear-dependent viscosity. Unlike power-law fluid, the Casson model is one of the non-Newtonian fluid models for which constitutive relationship holds at both low and high shear rates. (Hayat et al. (2015), Gireesha et al. (2015), Raju et al. (2016), Kuznetsov et al. (2014) and Yin et al. (1996)).

In the recent years, the study of magnetohydrodynamic (MHD) has gained considerable attention due to its practical applications in numerous technologies, including, MHD power generators, cooling of nuclear reactors, and construction of heat exchangers, installation of nuclear accelerators, blood flow measurement techniques and on the performance of several other systems employing electrically conducting fluids. On the other hand, magnetic nanofluids possess both the magnetic and liquid properties. Madhu et al. (2015) investigated MHD mixed convection stagnation-point flow of a non-Newtonian power-law nanofluid towards a stretching surface. Kishan et al. (2013) and Kishan et al. (2009) studied MHD heat transfer to non-Newtonian power-law fluids flowing over a wedge.

In unrestricted, the working capacity of the machines will also pivot on upon the effectiveness of the heat transfer rate of the liquids used. Customarily the factories will use water, transformer oil, and kerosene as the heat transfer liquids which do not possess sufficient thermal conductivity as the industries needed. Since the solid materials exhibit good thermal conductivity, a scientist namely Choi of ANL has made an attempt by adding nano-sized solid particles in the base fluids and discovered that thermal conductivity of the conventional fluids can be increased with the addition of solid nanoparticles like graphene, ferrite, titanium oxide etc. From that pioneering work on words, many investigations were perpetrated by the researchers of mechanical engineering owing to the vast applications of nanofluids (any fluid with solid nanoparticles) in heat transfer mechanism. Among them, Baby et al. (2011) are one to examine the heat transfer of liquids by dispersing graphene nanoparticles. Recently, Das et al. (2014) has given a comparative study between base fluids and nanofluids graphically. In this paper, the author used copper and aluminum oxide nanoparticles. Siddiq et al. (2009) found a mathematical model to characterize the bio convective flow of a nanofluid past a wavy cone. Then after, Khan et al. (2012) presented a numerical treatment for describing the heat and mass transfer effects on non-Newtonian nanofluid flows across a convective surface by making use of finite difference scheme. Nadeem et al. (2016) comparatively explored the flow behavior of fluids with nanoparticles.

Incited by the above information, so far no effort is made on the widening paper to the work of Gopal et al. (2017) to study the viscous and Joule's dissipation on Casson fluid over a chemically reacting stretching sheet with inclined magnetic field and multiple slips. The current work focus to fill this gap in the widening literature. Almost identical solutions are acquired and abbreviate ordinary differential equations are solved numerically using the Runge-Kutta-Fehlberg with the shooting method.

2. Mathematical formulation

Consider a steady, incompressible, two-dimensional boundary layer flow of a Casson fluid over an inclined permeable stretching sheet. The buoyancy forces are accountable for the flow. The velocity of the stretching sheet is appropriated form $\lambda u_w(x)$, with $\lambda > 0$ for a stretching surface, where $x-$ and $y-$ axes are measured along the stretching surface and normal to stretched surface respectively, and the flow is observed to $\lambda > 0$. It is also appropriated that the constant temperature and concentration at the surface of the sheet are T_∞ and C_∞, where the ambient fluid temperature and concentration are and the rheological equation of state for an anisotropic and incompressible flow of a Casson fluid is given by Ref. Eldabe et al. (1995). The mass, momentum, heat and concentration equations are given below,

$$u_x + v_y = 0, \tag{1}$$

$$uu_x + vu_y = v\left(1 + \frac{1}{\beta}\right)u_yy - \frac{\sigma B_0^2}{\rho}\sin^2\alpha + g\beta_T(T - T_\infty)\cos\alpha + g\beta(C - C_\infty)\cos\alpha - \frac{vu}{k^*}, \tag{2}$$

$$uT_x + vT_y = \alpha T_{yy} + \frac{v}{C_p}\left(1 + \frac{1}{\beta}\right)(u_y)^2 + \frac{\sigma B_0^2 u^2}{\rho C_p} - \frac{\partial q_r}{\partial y} + \frac{Q_0}{\rho C_p}(T - T_\infty), \tag{3}$$

$$uC_x + vC_y = D_B C_{yy} + \frac{D_T}{T_\infty}T_{yy} - k_0(C - C_\infty), \tag{4}$$

where u and v are the velocity component along the $x-$ and $y-$ axes respectively. T is the fluid temperature, C is the concentration, v is the kinematic viscosity of the fluid, α^* is the thermal diffusivity of the fluid, ρ is the density of the fluid, D_B is the mass diffusion, C_p is the specific heat at constant pressure, σ is the electric conductivity of the fluid, B_0 is the applied uniform magnetic field normal to the surface of the sheet, q_r is the radiative heat flux, Q_0 is the volumetric rate of heat generation or absorption, g is gravitational force, β_T is the thermal expansion coefficient, β_C is the solutal expansion coefficient, D_T is the thermophoresis diffusion coefficient, T_∞ ambient temperature, k^* is the permeability coefficient of porous medium, α is the inclination of the stretching sheet parameter and k_0 is respectively the constant chemical reaction rate.

Assume that Equations (1) - (4) are subjected to the boundary conditions are

$$u = \lambda u_w(x) + Lu_y, v = v_0, T = T_w + ST_y, C = C_w + KC_y \text{ at } y = 0,$$

$$u \to 0, T \to T_\infty, C \to C_\infty \text{ as } y \to \infty, \tag{5}$$

where $u_w(x) = ax$ and a is the positive constant. By utilizing Rosseland approximation in the energy equation (3) reduced to

$$uT_x + vT_y = \alpha^*\left(1 + \frac{16\sigma^* T_\infty^3}{3kk^*}\right)T_{yy} + \frac{Q_0}{\rho C_p}(T - T_\infty) + \frac{v}{C_p}\left(1 + \frac{1}{\beta}\right)(u_y)^2 + \frac{\sigma B_0^2 u^2}{\rho C_p}, \tag{6}$$

σ^* is the Stefan-Boltzmann constant, k is the thermal conductivity and k^* is the mean absorption coefficient. We observe for a similarity solution of Equations (1), (2), (4) and (6) of the following form:

$$\psi = \sqrt{avx}f(\eta), \theta(\eta) = \frac{T - T_\infty}{T_w - T_\infty}, \phi(\eta) = \frac{C - C_\infty}{C_w - C_\infty}, \eta = y\sqrt{\frac{a}{v}}, \tag{7}$$

where $\psi(x, y)$ is the stream function, with these stream functions defined as $u = \psi_y$ and $v = -\psi_x$. Thus, we get

$$u = axf_\eta, v = -\sqrt{a\upsilon}f(\eta). \tag{8}$$

f_η denotes the differentiation with respective η. We take the dimensionless parameter S, δ, γ and χ are denote as

$$S = -\frac{v_0}{\sqrt{a\upsilon}}, \delta = \sqrt{\frac{a}{\upsilon}}L, \gamma = \sqrt{\frac{a}{\upsilon}}S, \chi = \sqrt{\frac{a}{\upsilon}}K, \tag{9}$$

where L is the velocity slip length, $S > 0$ corresponds to suction, $S < 0$ for injection δ is the velocity slip parameter, γ is the thermal slip/jump parameter and β is the mass slip parameter.

Substituting (7) into Equations (2), (4) and (6), we obtain the following ordinary differential equations

$$\left(1 + \frac{1}{\beta}\right)f_{\eta\eta\eta} + f_{\eta\eta}f - (f_\eta)^2 + (Gr\theta + Gc\phi)\cos(\alpha) - (M\sin^2(\alpha) + K)f_\eta = 0, \tag{10}$$

$$\frac{1}{Pr}\left(1 + \frac{4R}{3}\right)\theta_{\eta\eta} + f\theta_\eta + Q\theta + Ec\left(1 + \frac{1}{\beta}\right)(f_{\eta\eta})^2 + J(f_\eta)^2 = 0, \tag{11}$$

$$\frac{1}{Sc}\phi_{\eta\eta} + \frac{Nt}{Nb}\theta_{\eta\eta} + f\phi_\eta - \tau\phi = 0. \tag{12}$$

The dimensionless boundary conditions are given below

$$f(0) = S, f_\eta(0) = \lambda + \delta f_{\eta\eta}(0), \theta(0) = 1 + \gamma\theta_\eta(0), \phi(0) = 1 + \chi\phi_\eta(0),$$

$$f_\eta(0) \to 0, \theta(\infty) \to 0, \phi(\infty) \to 0. \tag{13}$$

The dimensionless parameter denotes as Pr the Prandtl number, Sc is the Schmidt number, M is the magnetic parameter, R is the radiation parameter, Gr is thermal Grashof number, Gc is solutal Grashof number, Q the heat source/sink parameter, K is the Permeability parameter, τ Chemical reaction parameter, Ec Eckert number and J Joule heating parameter which are defined as

$$Pr = \sqrt{\frac{\upsilon}{\alpha}}, Sc = \frac{\upsilon}{D_B}, M = \frac{\sigma B_0^2}{\rho a}, R = \frac{4\sigma^* T_\infty^3}{kk^*}, Gr = \frac{g\beta_T(T_w - T_\infty)}{a^2 x}, Gc = \frac{g\beta_C(C_w - C_\infty)}{a^2 x},$$

$$Q = \frac{Q_0}{a\rho C_p}, K = \frac{\upsilon}{k^* a}, \tau = \frac{k_0}{a}, Ec = \frac{u_w^2}{C_p(T_w - T_\infty)}, J = \frac{\sigma B_0^2}{\rho C_p(T_w - T_\infty)}. \tag{14}$$

We also computed the physical quantities values of skin friction coefficient C_{f_x}, the local Nusselt number Nu_x and local Sherwood number Sh_x, which are described as

$$C_{f_x} = \frac{\tau_w}{\rho u_w^2(x)}, Nu_x = \frac{xq_w}{k(T_w - T_\infty)}, Sh_x = \frac{xq_m}{D_B(C_w - C_\infty)}, \tag{15}$$

where τ_w, q_w and q_m are the skin friction or shear stress, heat flux and mass flux from the sheet, which are given by

$$\tau_w = \mu(u_y)_{y=0}, q_w = -(T_y)_{y=0} + (q_r)_{y=o}, q_m = -D_B(C_y)_{y=0}, \tag{16}$$

where μ is the dynamic viscosity of the fluid. Utilizing (7), (15) and (16), we get

$$Re_x^{\frac{1}{2}}C_{f_x} = \left(1 + \frac{1}{\beta}\right)f_{\eta\eta}(0), Re_x^{\frac{-1}{2}}Nu_x = -\theta_\eta(0), Re_x^{\frac{-1}{2}}Sh_x = -\phi_\eta(0). \tag{17}$$
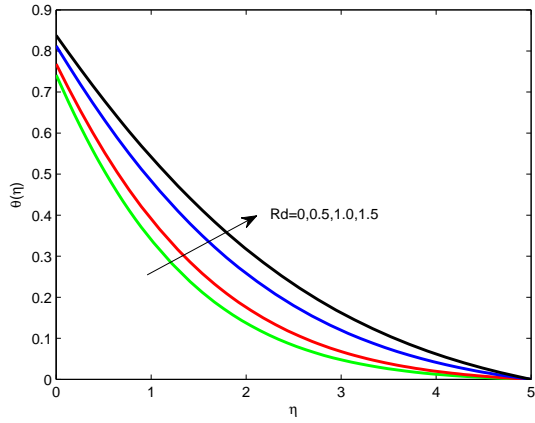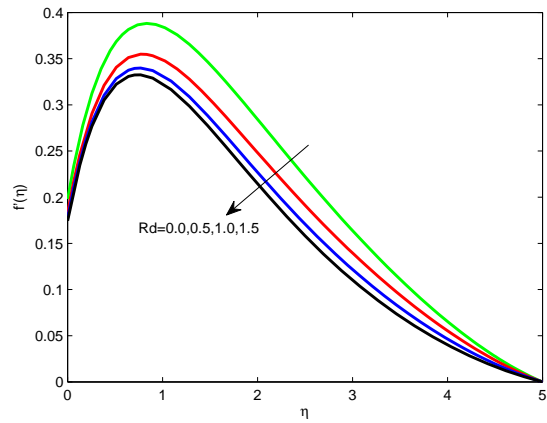
Figure 1. Impact of Rd on $f^{'}(\eta)$

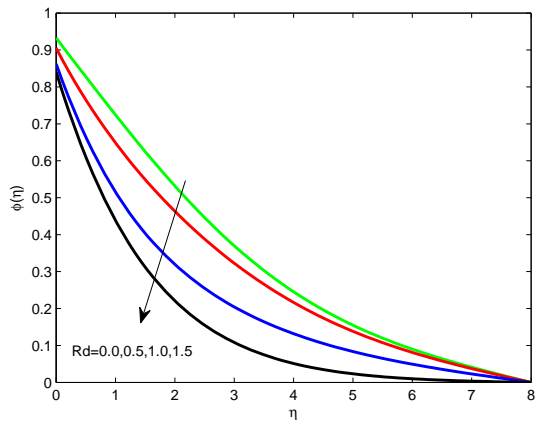**Figure 2.** Impact of Rd on $\theta(\eta)$

Figure 3. Impact of Rd on $\phi(\eta)$
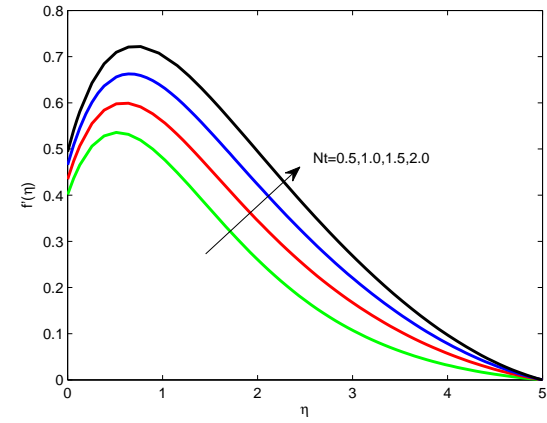
Figure 4. Impact of Nt on $f^{'}(\eta)$
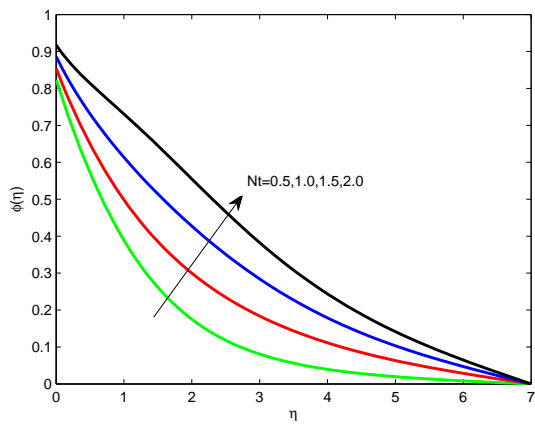
Figure 5. Impact of Nt on $\phi(\eta)$

Figure 6. Impact of Nb on $f^{'}(\eta)$

Applications and Applied Mathematics: An International Journal (AAM), Vol. 14 [2019], Iss. 4, Art. 9

AAM: Intern. J., Special Issue No. 4 (March 2019)   111
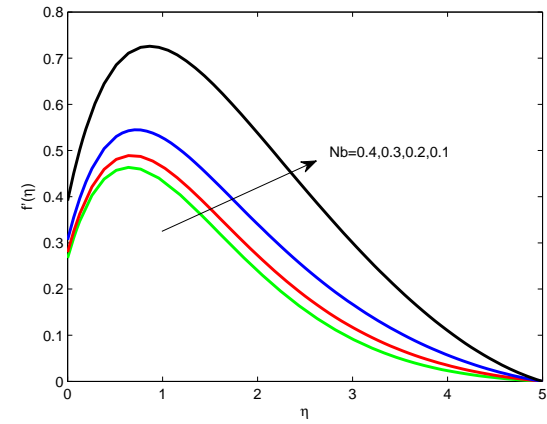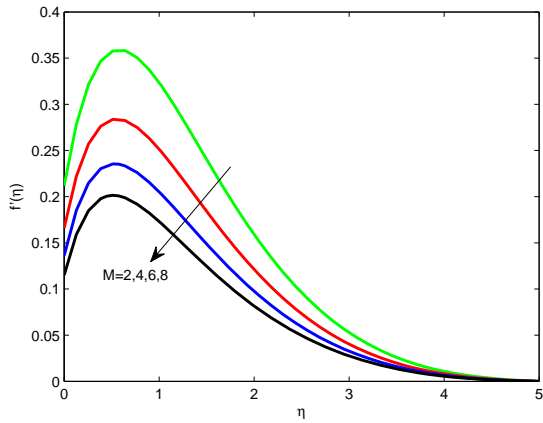
Figure 7. Impact of M on $f^{'}(\eta)$
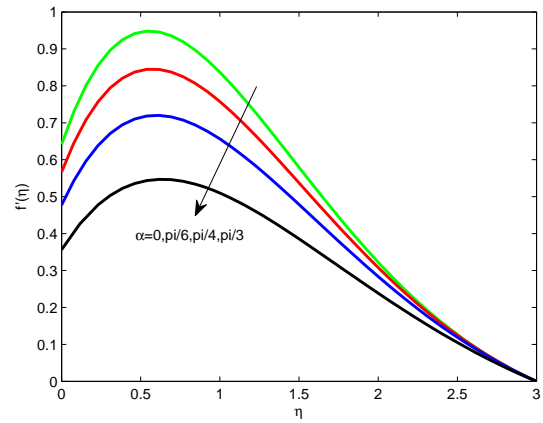
Figure 8. Impact of α on $f^{'}(\eta)$
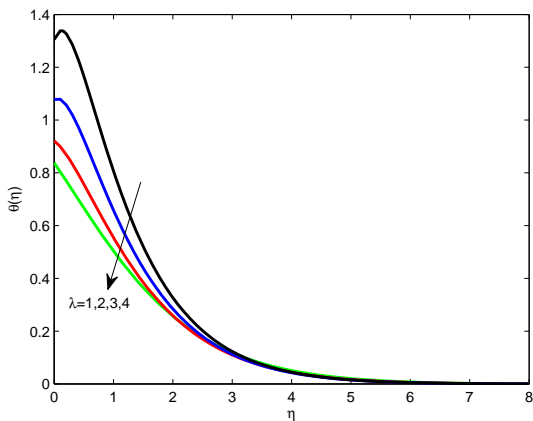
Figure 9. Impact of λ on $\theta(\eta)$
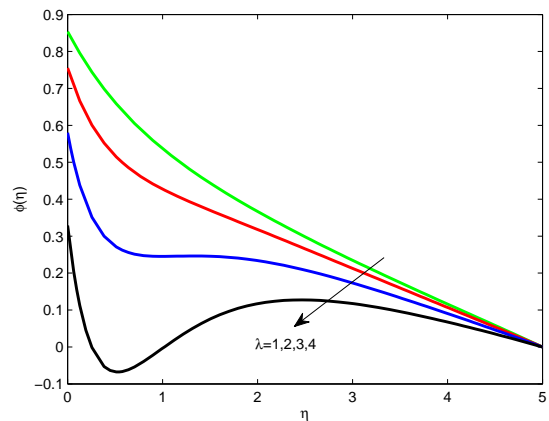
Figure 10. Impact of λ on $\phi(\eta)$
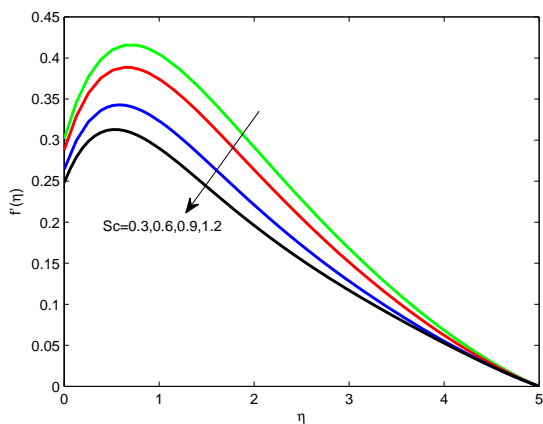
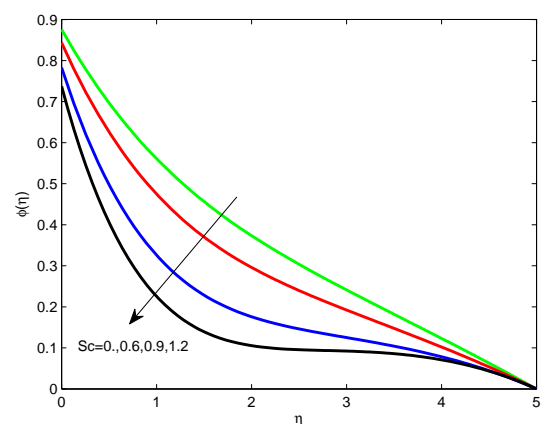

Figure 11. Impact of Sc on $f^{'}(\eta)$

Figure 12. Impact of Sc on $\phi(\eta)$
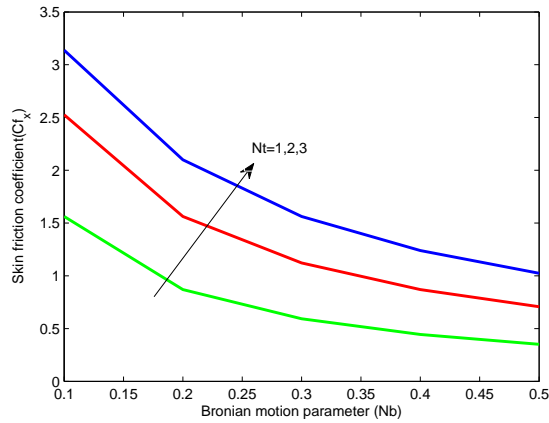
Figure 13. Impact of Nb and Nt on C_{f_x}
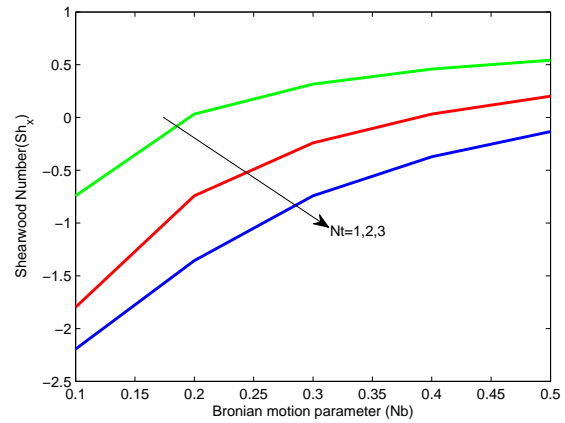
Figure 14. Impact of Nb and Nt on Sh_x
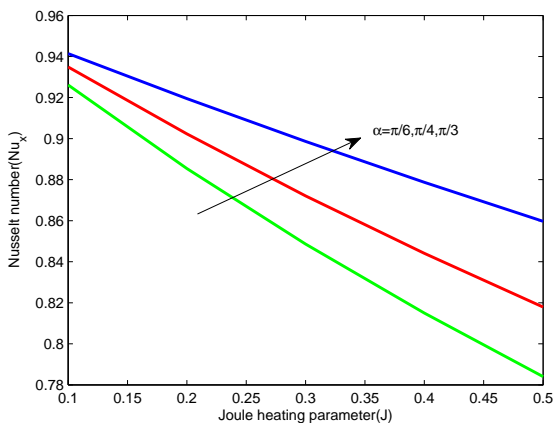
Figure 15. Impact of J and α on Nu_x
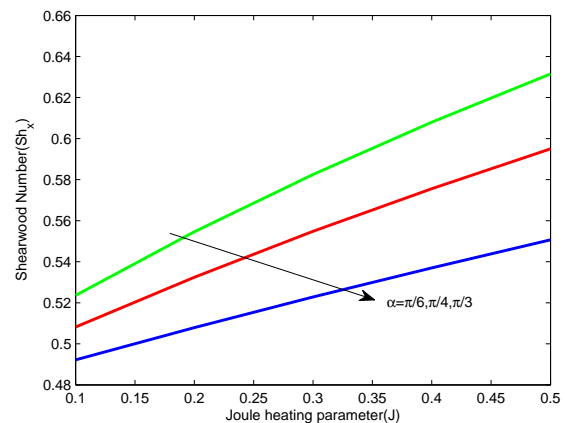
Figure 16. Impact of J and α on Sh_x

3.   Results and Discussion

The dimensionless governing Equations (9) - (12) are solved using the Runge-Kutta and Newtons methods with the support of the boundary condition (Equation (14)). In order to simulate the problem, the determine values of dimensionless parameters are utilized such as $\alpha = \frac{\pi}{3}; \beta = 1.5; \gamma = 0.5; \delta = 0.5; \lambda = 0.2; \chi = 0.3; \Gamma = 0.4; Gc = 5; Gr = 2; M = 0.5; K = 0.6; Pr = 0.72; R = 0.2; Q = 0.3; Ec = 0.2; J = 0.3; Sc = 0.5; Nb = 2; Nt = 2.5; S = 1$. These values are considered fixed in the entire computation except the variation in respective figures. The contemporary numerical results expose the effect of various dimensionless variables such as Brownian motion parameter, thermophoresis parameter, Prandtl number, Radiation, Joule heating parameter, and magnetic field parameter on the common profile (velocity, temperature and concentration). The effects of these dimensionless parameters on skin friction coefficient, local Nusselt number and Sherwood number are summarized in Figures 13 - 16.

The effects of radiation parameter on velocity, temperature and concentration fields are demonstrated in Figures 2 - 4. It is observed that arising in the values of thermal radiation parameter

Applications and Applied Mathematics: An International Journal (AAM), Vol. 14 [2019], Iss. 4, Art. 9

AAM: Intern. J., Special Issue No. 4 (March 2019)   113

enhances in velocity, temperature and concentration distributions. Physically, increasing in thermal radiation parameter heat to the flow near the surface and move the concentration particles to cooler areas from the surface. Due to this we observed reduction in velocity and concentration hike in the temperature fields.

The effects of thermophoresis Nt and Brownian motion Nb parameter on velocity and concentration profile are plotted in Figures 5 - 7. It is observed that an enhancement in the velocity and concentration boundary layer for increasing values of thermophoresis parameter (Figures 5 and 6). In contrast, velocity increases for increasing the values of Brownian motion parameter (Figure 7). This fact indicates that the different materials have various values of Nb and Nt. Figures 8 - 9 illustrate the variation of M and α on velocity profile, respectively. Figure 8 depicts that reducing values of M reduction the Magnetic parameter and enhances the magnetic capacity of fluid, accordingly dimensionless velocity dropped. Clearly, Figure 9 shows that the fluid velocity is reducing with the inclination angle parameter.

When the stretching parameter λ is arise then the behavior of temperature and concentration remains similar as compared to different values of stretching parameter λ. Figure 10 is sketched for various values of stretching parameter λ from this figure, it can noticed that when the stretching parameter arise then it is strongly beneficial in decelerating the fluid flow. It can be observed from Figure 11 that when the stretching parameter λ arises then the boundary layer thickness decreases. Conduct of Schmidt number Sc on velocity and concentration profiles are sketched in Figures 12 - 13. Conduct of velocity, concentration enhances for larger Schmidt number. In fact Schmidt number is the ratio of momentum diffusivity to mass diffusivity. Here larger values of Schmidt number correspond to small diffusivity of velocity and concentration distribution reduction.

In Figures 14 - 15, the dimensionless Skin fraction coefficient and Sherwood number are plotted along with thermophoresis parameter Nt by varying the Brownian motion parameter Nb these graphs reveal that the rate of Skin fraction coefficient arise in response to a arise in thermophoresis parameter and Sherwood number reduction with the thermophoresis parameter. Figures 16 - 17 gives the plots of Nusselt number and Sherwood numbers augments the Joule heating parameter J for different values of inclination angle parameter α. It is observed that the Nusselt number arise with arise inclination angle parameter α and Sherwood numbers reduces with the inclination angle parameter α and Joule heating parameter J.

Table 1 displays the varying of skin friction, Nusselt number and Sherwood number with revising values of $M, Pr, Nb, Nt, J, \alpha, \beta, \gamma$ and δ. It is clear that the skin friction coefficients are reassured with raising values of the Prandtl number, thermophoresis, Casson parameter, velocity slip parameter and the rest of the parameters are opposite behavior. In the Nusselt number arising with the raising Joule heating parameter, thermal slip parameter and the Nusselt number decreasing with the raising parameters are Magnetic parameter, Prandtl number, Brownian motion, inclined parameter. Here Sherwood number are boosting with the Nb, J, β and decreasing with the parameters $M, Pr, Nt, \alpha, \gamma$ and δ.

Table 1. Varying in Skin friction coefficient, Nusselt number and Sherwood number for divergent values of $\lambda = 0.2; \chi = 0.3; \Gamma = 0.4; Gc = 5; Gr = 2; K = 0.6; R = 0.2; Q = 0.3; Ec = 0.2; Sc = 0.5; S = 1$.

M	Pr	Nb	Nt	J	α	β	γ	δ	$\left(1+\frac{1}{\beta}\right)f''(0)$	$-\theta'(0)$	$-\phi'(0)$
1	0.7	0.5	0.2	0.3	$\frac{\pi}{4}$	1	0.5	0.2	0.217574	0.432128	0.451893
2									0.128458	0.436076	0.440687
3									0.049668	0.438544	0.432229
	0.5								0.296824	0.506367	0.364580
	1.0								0.381841	0.735878	0.045981
	1.5								0.432251	0.897214	0.020605
		0.6							0.226654	0.370289	0.545230
		1.2							0.184508	0.370758	0.595085
		1.8							0.170388	0.370772	0.611899
			0.7						0.151053	0.370672	0.634987
			1.4						0.159939	0.370735	0.624368
			2.1						0.168834	0.370769	0.613752
				0.4					0.206846	0.379412	0.562619
				0.8					0.202083	0.344495	0.591935
				1.2					0.197443	0.310402	0.620590
					$\pi/6$				0.412179	0.350670	0.599095
					$\pi/4$				0.204448	0.361847	0.577362
					$\pi/3$				0.065907	0.369944	0.554419
						1			0.200109	0.360345	0.576826
						2			0.201306	0.362643	0.577685
						3			0.202273	0.363482	0.578045
							0.2		0.215444	0.377658	0.581986
							0.4		0.194299	0.347336	0.573122
							0.6		0.176167	0.321617	0.565610
								0.1	-0.081710	0.439812	0.391952
								0.3	-0.062082	0.440163	0.391051
								0.5	-0.050067	0.440365	0.390517

4.   Conclusion

The inclined magnetic field, thermophoresis and Brownian motion on Casson fluid over a stretching sheet in the presence of velocity, thermal and concentration slip conditions are investigated. Mathematical solutions are developed for various physical quantities like velocity, temperature, and concentration. The main lists of the findings are as follows.

- The effect of thermophoresis parameter Nt is to arise the velocity while enhances the concentration profiles.
- The radiative heat, viscous dissipation and Joule heating aspects are constructive for the growth

Applications and Applied Mathematics: An International Journal (AAM), Vol. 14 [2019], Iss. 4, Art. 9

AAM: Intern. J., Special Issue No. 4 (March 2019) 115

of thicknesses of the thermal boundary layer of Casson fluid.

- The velocity profiles arising with the arising of Brownian motion Nb these velocity profile reduction Rd with radiation parameter α, inclination angle parameter and Schmidt number Sc where as it they increase.
- The velocity reduction with respect to magnetic parameter M.
- Skin fraction coefficient function arising and Sherwood number reducing with Nb and Nt Nusselt number is an arising function of J and α.

Acknowledgments

REFERENCES

Baby, T.T. and Ramaprabhu, S. (2011). Enhanced convective heat transfer using graphene dispersed nanofluids, Nanoscale Res. Lett. Vol. 6, pp. 289–296.

Das, K. (2014). Flow and heat transfer characteristics of nanofluids in a rotating frame, Alex. Eng. J, Vol. 53, pp. 757–766.

Eldabe, NTM. and Salwa, MGE. (1995). Heat transfer of MHD non-Newtonian Casson fluid flow between two rotating cylinder. J. Phy Soc Jpn, Vol. 64, pp. 41–64.

Gireesha, B.J., Gorla, RSR. and Mahanthesh, B. (2015). Effect of suspended nanoparticles on three dimensional MHD flow, heat and mass transfer of radiating Eyring-Powell fluid over a stretching sheet, J Nanofluids, Vol. 4, pp. 474–84.

Gopal, D., Kishan, N. and Raju, C.S.K (2017). Viscous and Joule's dissipation on Casson fluid over a chemically reacting stretching sheet with inclined magnetic field and multiple slips, IMU, Vol. 9, pp. 154–160.

Hayat, T., Muhammad, T., Shehzad, SA., Chen, G.Q. and Abbas IA. (2015). Interaction of magnetic field in flow of Maxwell nanofluid with convective effect, J Magn Magn Mater, Vol. 385, pp. 48–55.

Hayat, T., Qayyum, S., Alsaedi, A. and Asghar, S. (2017). Radiation effects on the mixed convection flow induced by an inclined stretching cylinder with non-uniform heat source/sink, PLoS ONE, Vol. 12, pp. 75–84.

Hayat, T., Qayyum, S. and lsaedi, A. (2017). Mechanisms of nonlinear convective flow of Jeffrey nanofluid due to nonlinear radially stretching sheet with convective conditions and magnetic field, Results Phy, Vol. 23, pp. 41–51.

Hsiao, KL. (2017). Combined electrical MHD heat transfer thermal extrusion system using Maxwell fluid with radiative and viscous dissipation effects, Appl Therm Eng, Vol. 112, pp. 1281–1289.

Hsiao, KL. (2017). Micropolar nanofluid flow with MHD and viscous dissipation effects towards a stretching sheet with multimedia feature, Int J Heat Mass Transfer, Vol. 11, pp. 83–90.

Khan, M., Irfan, M., Khan, WA. and Ahmad, L. (2017). Modeling and simulation for 3D magneto Eyring-Powell nanomaterial subject to nonlinear thermal radiation and convective heating, Results Phys, Vol. 7, pp. 1899–1906.

Khan, M., Irfan, M. and Khan, WA. (2017). Impact of nonlinear thermal radiation and gyrotactic microorganisms on the magneto-Burgers nanofluid, Int J Mech Sci, Vol 130, pp. 375–385.

Khan, W.A. and Gorla, R.S.R. (2012). Heat and mass transfer in power-law nanofluids over a non-isothermal stretching wall with convective boundary condition, J. Heat Transf, Vol. 134, pp. 112001.

Kishan, N. and Amrutha, P. (2009). MHD heat transfer to non-Newtonian power-law fluids flowing over a wedge with viscous dissipation, IJAME, Vol. 14, pp. 965–987.

Kishan, N. and Kavitha, P. (2013). Quasi linearization approach to MHD heat transfer to non-newtonian power-law fluids flowing over a wedge with heat source/sink in the presence of viscous dissipation, IJMCAR, Vol. 3, pp. 15–28.

Kuznetsov, A.V., and Nield, D.A. (2014). Natural convective boundary-layer flow of a nanofluid past a vertical plate: A revised model, Int. J. Theor. Sci, Vol. 77, pp. 126–129.

Madhu, M. and Kishan, N. (2015). Magnetohydrodynamic mixed convection stagnation-point flow of a power-law non-Newtonian nanofluid towards a stretching surface with radiation and heat source/sink, J. Fluids, ID634186.

Nadeem, S., Khan, A.U. and Saleem, S. (2016). A comparative analysis on different nanofluid models for the oscillatory stagnation point flow, Eur. Phys. J. Plus. pp. 16261–16269

Raju, C.S.K., Ibrahim, S.M., Anuradha, S. and Priyadharshini, P. (2016). Bio-convection on the nonlinear radiative flow of a Carreau fluid over a moving wedge with suction or injection, The Eur. Phys. J. Plus, Vol.13, pp. 16409–16417

Siddiq, S., Hina, G.E., Begum, N., Saleem, S., Hossain, M.A. and Gorla, R.S.R. (2016). Numerical solutions of nanofluid bioconvection due to gyrotacticmicroorganisms along a vertical wavy cone, Int. J. Heat Mass Transf., Vol. 101, pp. 608–613.

Wang, S. and Tan, WC. (2011). Stability analysis of Soret driven double-diffusive convection of Maxwell fluid in a porous medium, Int J Heat Fluid Flow, Vol. 32, pp. 88–94.

Yih, K.A. (1996). Forced convection flow adjacent to a nonisothermal wedge, Int. Commun. Heat Mass Transf, Vol. 26, pp. 819–827.